

# Structural Studies of Inositol 1,4,5-Trisphosphate Receptor COUPLING LIGAND BINDING TO CHANNEL GATING\*<sup>‡</sup>

Received for publication, May 1, 2010, and in revised form, September 1, 2010. Published, JBC Papers in Press, September 15, 2010, DOI 10.1074/jbc.M110.140160

Jenny Chan<sup>‡</sup>, Haruka Yamazaki<sup>§¶</sup>, Noboru Ishiyama<sup>‡</sup>, Min-Duk Seo<sup>‡</sup>, Tapas K. Mal<sup>‡</sup>, Takayuki Michikawa<sup>§¶</sup>,  
Katsuhiko Mikoshiba<sup>§¶1</sup>, and Mitsuhiko Ikura<sup>‡2</sup>

From the <sup>‡</sup>Division of Signaling Biology, Ontario Cancer Institute and Department of Medical Biophysics, University of Toronto, Toronto, Ontario M5G 1L7, Canada, the <sup>§</sup>Laboratory for Developmental Neurobiology, Brain Science Institute, RIKEN, Saitama 351-0198, Japan, and the <sup>¶</sup>Calcium Oscillation Project, Solution Oriented Research for Science and Technology, Japan Science and Technology Agency, Saitama 322-0012, Japan

The three isoforms of the inositol 1,4,5-trisphosphate receptor (IP<sub>3</sub>R) exhibit distinct IP<sub>3</sub> sensitivities and cooperativities in calcium (Ca<sup>2+</sup>) channel function. The determinants underlying this isoform-specific channel gating mechanism have been localized to the N-terminal suppressor region of IP<sub>3</sub>R. We determined the 1.9 Å crystal structure of the suppressor domain from type 3 IP<sub>3</sub>R (IP<sub>3</sub>R<sub>3SUP</sub>, amino acids 1–224) and revealed structural features contributing to isoform-specific functionality of IP<sub>3</sub>R by comparing it with our previously determined structure of the type 1 suppressor domain (IP<sub>3</sub>R<sub>1SUP</sub>). The molecular surface known to associate with the ligand binding domain (amino acids 224–604) showed marked differences between IP<sub>3</sub>R<sub>3SUP</sub> and IP<sub>3</sub>R<sub>1SUP</sub>. Our NMR and biochemical studies showed that three spatially clustered residues (Glu-20, Tyr-167, and Ser-217 in IP<sub>3</sub>R<sub>1</sub> and Glu-19, Trp-168, and Ser-218 in IP<sub>3</sub>R<sub>3</sub>) within the N-terminal suppressor domains of IP<sub>3</sub>R<sub>1SUP</sub> and IP<sub>3</sub>R<sub>3SUP</sub> interact directly with their respective C-terminal fragments. Together with the accompanying paper (Yamazaki, H., Chan, J., Ikura, M., Michikawa, T., and Mikoshiba, K. (2010) *J. Biol. Chem.* 285, 36081–36091), we demonstrate that the single aromatic residue in this region (Tyr-167 in IP<sub>3</sub>R<sub>1</sub> and Trp-168 in IP<sub>3</sub>R<sub>3</sub>) plays a critical role in the coupling between ligand binding and channel gating.

The inositol 1,4,5-trisphosphate (IP<sub>3</sub>)<sup>3</sup> receptors (IP<sub>3</sub>Rs) are tetrameric intracellular Ca<sup>2+</sup> release channels on the endoplasmic

membrane that are activated by the ligand IP<sub>3</sub>. In mammals, the IP<sub>3</sub>R family consists of three genes, which encode for isoforms type 1 (IP<sub>3</sub>R<sub>1</sub>), type 2 (IP<sub>3</sub>R<sub>2</sub>), and type 3 (IP<sub>3</sub>R<sub>3</sub>) (1). The full-length isoforms are 60–70% identical in primary sequence, with the N-terminal ligand-binding and C-terminal channel domains sharing the highest similarity (2). IP<sub>3</sub>R is ubiquitously expressed, and most cells express more than one IP<sub>3</sub>R isoform (3–5).

IP<sub>3</sub>R<sub>1</sub> is widely expressed in the central nervous system, in particular the cerebellar Purkinje cells (6). The importance of IP<sub>3</sub>R<sub>1</sub> in embryonic development is demonstrated by the fact that the majority of IP<sub>3</sub>R<sub>1</sub> knock-out mice die *in utero* (7). IP<sub>3</sub>R<sub>1</sub>-null animals that survive until birth have 40% brain sizes and 50% body mass compared with wild type littermates. In contrast, neither IP<sub>3</sub>R<sub>2</sub> nor IP<sub>3</sub>R<sub>3</sub> knock-out mice display any abnormal phenotype (8). However, double IP<sub>3</sub>R<sub>2</sub><sup>-/-</sup>-IP<sub>3</sub>R<sub>3</sub><sup>-/-</sup> knock-out animals show defects in exocrine functions. For example, saliva production is greatly reduced in double knock-out mice as a consequence of defective IP<sub>3</sub>-mediated Ca<sup>2+</sup> release (8).

Although functional differences among IP<sub>3</sub>R isoforms *in vivo* remain unclear, *in vitro* studies of IP<sub>3</sub>R have revealed that one of the most significant differences between the isoforms is in their IP<sub>3</sub> binding affinities. IP<sub>3</sub>R<sub>2</sub> exhibits the highest IP<sub>3</sub> binding affinity, followed by IP<sub>3</sub>R<sub>1</sub> and then IP<sub>3</sub>R<sub>3</sub> (*K<sub>d</sub>* = 5.9, 28.6, and 294 nM, respectively) (9, 10). Using chimeric proteins, we have shown that different IP<sub>3</sub> binding affinities of IP<sub>3</sub>R isoforms are not solely dependent on the ligand binding core (IP<sub>3</sub>R<sub>CORE</sub>; amino acids 224–578) but also involve the suppressor domain (IP<sub>3</sub>R<sub>SUP</sub>; amino acids 1–223) (9). The molecular mechanism underlying these isoform-specific affinities is not well understood, but recent studies suggest that distinct IP<sub>3</sub> sensitivities of the three isoforms are a product of the suppressor and ligand binding domain interaction (9).

Earlier biochemical studies (11) show that there is a direct coupling between the N and C termini in IP<sub>3</sub>R<sub>1</sub>, believed to occur in an intermolecular manner (*i.e.* aa 1–340 of the N-terminal fragment of one subunit interact with sites located between aa 2418 and 2749 of the C-terminal fragment of an adjacent subunit). Introduction of mutations within a cytoplasmic loop that connects transmembrane helices 4 and 5 in the C-terminal fragment (aa 2418–2437; M4-M5 linker) prevents the co-immunoprecipitation of N and C termini, suggesting that this region is involved in the N-terminal-to-C-terminal

\* This work was supported by a Heart and Stroke Foundation of Ontario (to M. I.), a Canadian Institutes of Health Research (CIHR) doctoral award (to J. C.) and a CIHR postdoctoral fellowship (to N. I.) and was supported by grants from the Special Postdoctoral Researchers Program in RIKEN (to H. Y.) and Ministry of Education, Science, Sports, and Culture of Japan Grants 20370054 (to T. M.) and 20220007 (to K. M.).

The atomic coordinates and structure factors (code 3JRR) have been deposited in the Protein Data Bank, Research Collaboratory for Structural Bioinformatics, Rutgers University, New Brunswick, NJ (<http://www.rcsb.org/>).

<sup>‡</sup> The on-line version of this article (available at <http://www.jbc.org>) contains supplemental Figs. 1–6.

<sup>1</sup> To whom correspondence may be addressed: Laboratory for Developmental Neurobiology, RIKEN Brain Science Institute, 2-1 Hirosawa, Wako-shi, Saitama 351-0198, Japan. Tel.: 81-48-467-9745; Fax: 81-48-467-9744; E-mail: mikosiba@brain.riken.jp.

<sup>2</sup> Holder of a Canadian Research Chair in Cancer Structural Biology. To whom correspondence may be addressed: Ontario Cancer Institute, University of Toronto, MaRS Toronto Medical Discovery Tower, Rm. 4-804, 101 College St. Toronto, Ontario M5G 1L7, Canada. Tel.: 416-581-7550; Fax: 416-581-7564; E-mail: mikura@uhnres.utoronto.ca.

<sup>3</sup> The abbreviations used are: IP<sub>3</sub>, inositol 1,4,5-trisphosphate; IP<sub>3</sub>R, IP<sub>3</sub> receptor; aa, amino acids; TCEP, tris(2-carboxyethyl)phosphine; IPTG, isopropyl 1-thio-β-D-galactopyranoside; HSQC, heteronuclear single quantum coherence.

intersubunit interaction (N-C interaction). The M4-M5 linker has been implicated in IP<sub>3</sub>R gating function because mutations to this region inhibit channel activity (12). Moreover, we have previously demonstrated that deletion of the suppressor domain abolishes channel activity while simultaneously increasing IP<sub>3</sub> binding affinity (13), thus suggesting the suppressor domain is essential to IP<sub>3</sub>R gating function. Despite this evidence of the functional significance of the suppressor domain in the channel regulation, little is known about the structural determinants responsible for the N-C interaction of IP<sub>3</sub>R.

In our accompanying paper (31), we report the identification of critical amino acid residues in the suppressor domain for IP<sub>3</sub>R channel gating function. Specifically, a single mutation of Tyr-167 to alanine in IP<sub>3</sub>R1 or the corresponding mutation in IP<sub>3</sub>R3 (W168A) was sufficient to abolish channel activity, suggesting that this residue is crucial to the gating mechanism of IP<sub>3</sub>R. In this paper, we report structural evidence for the significance of this aromatic residue in the physical contact between the N-terminal suppressor domain and the C-terminal channel domain. We determined the high resolution crystal structure of the suppressor domain from type 3 IP<sub>3</sub>R and characterized the interaction between the suppressor domain and synthetic peptides of the M4-M5 linker by NMR and biochemical approaches. Our structural data provide further evidence for the involvement of not only the aromatic residue (*i.e.* Trp-168 in IP<sub>3</sub>R3) but also some neighboring residues within the suppressor domain in this functionally essential interaction. This region responsible for the interaction with the C terminus of the receptor is adjacent to but distinct from the sites of IP<sub>3</sub> binding modulation and IP<sub>3</sub> binding core interaction.

## EXPERIMENTAL PROCEDURES

**Expression and Protein Purification**—Mouse IP<sub>3</sub>R3<sub>SUP</sub> (aa 1–224) was expressed as an N-terminal tagged GST fusion protein in BL21-CodonPlus(DE3)-RIL *Escherichia coli* strain (Stratagene). Freshly transformed cells were first grown in 4 liters of LB medium at 37 °C until A<sub>600</sub> reached ~0.6. Cells were then harvested, washed by resuspending in M9 medium, harvested again, and then transferred into 1 liter of minimal M9 medium supplemented with 1 g/liter [<sup>15</sup>N]NH<sub>4</sub>Cl and/or 2 g/liter [<sup>13</sup>C<sub>6</sub>]glucose (Cambridge Isotope Laboratories). Additionally, for triple resonance experiments, the protein was deuterated by growing cells in 99% [<sup>2</sup>H]D<sub>2</sub>O-based M9 medium. Cell cultures were typically grown overnight at 15 °C following the addition of IPTG (0.5 mM final concentration). Cells were harvested by centrifugation and resuspended in ice-cold lysis buffer (20% (v/v) glycerol, 20 mM Tris-HCl, pH 8.4, 500 mM NaCl, 0.2% Nonidet P-40, 10 mM DTT, 10 μg/ml DNase I, EDTA-free protease inhibitor mixture (Roche Applied Science)). Cells were lysed by sonication, and the soluble lysate fraction was applied to a pre-equilibrated glutathione-Sepharose 4B resin (GE Healthcare) for affinity purification. The eluent was supplemented with 200 units of thrombin (Sigma) and subjected to dialysis overnight at 4 °C into 2 liters of dialysis buffer (3% (v/v) glycerol, 20 mM Tris-HCl, pH 8.4, 300 mM NaCl, 2 mM CaCl<sub>2</sub>, 0.5 mM TCEP). The sample was loaded onto a Superdex 75 gel filtration column (GE Healthcare). Eluted

protein fractions in S75 buffer (3% (v/v) glycerol, 15 mM Tris-HCl, pH 7.1, 300 mM NaCl, 2 mM TCEP) were collected and pooled. Using a 30 kDa cut-off Amicon Ultra concentration device (Millipore) the purified protein was concentrated to ~1 mM for NMR experiments. For crystallography, freshly transformed BL21-CodonPlus(DE3)-RIL *E. coli* cells (Stratagene) were used to express mouse IP<sub>3</sub>R3<sub>SUP</sub> (aa 1–224) as an N-terminally tagged GST fusion protein in 2 liters of LB medium at 37 °C. Protein expression was induced by a 0.5 mM final concentration of IPTG. Following growth overnight, cells were harvested by centrifugation, and protein purification was performed as described above. Amino acid mutations were introduced using the QuikChange site-directed mutagenesis kit (Stratagene). Mutant constructs were expressed and purified as above.

**Crystallography**—Crystals of IP<sub>3</sub>R3<sub>SUP</sub>, which was concentrated to 10 mg/ml, were grown by hanging drop vapor diffusion at 22 °C by combining 2 μl of protein with an equal volume of reservoir solution (100 mM HEPES, pH 7.6, 150 mM NaCl, 14% PEG 4000, 2 mM TCEP, 1% dioxane, 50 mM EDTA). Crystal clusters appeared within 2 weeks, and following 2–3 rounds of microseeding, single platelike crystals with dimensions 0.2 × 0.1 × 0.02 mm were obtained. They were flash-cooled in Paratone-N. Two rounds of annealing improved diffraction, and native data were collected at 100 K on a 19-BM beam line at the Advanced Photon Source Synchrotron facility (Argonne, IL). Data processing was carried out with HKL2000 (14). Crystals belonged to the space group C2 with cell dimensions *a* = 79.4 Å, *b* = 59.9 Å, *c* = 111.4 Å, β = 97.88° with two molecules in the asymmetric unit. Phase information was obtained by molecular replacement using the mouse IP<sub>3</sub>R1<sub>SUP</sub> crystal structure (Protein Data Bank code 1XZZ) as the search model. Refinement was carried out in CNS (15), and manual model building was performed with Coot (16). Electrostatic potentials were calculated using APBS (17).

**Nuclear Magnetic Resonance**—NMR spectra were recorded at 25 °C using a 600-MHz Varian INOVA spectrometer or an 800-MHz Bruker spectrometer. <sup>1</sup>H-<sup>15</sup>N heteronuclear single quantum coherence (HSQC) spectra were measured on a uniformly <sup>15</sup>N-labeled sample. HNCACB (18) and CBCA(CO)NH (19) triple resonance experiments were recorded at a protein concentration of ~1 mM using uniformly <sup>2</sup>H-, <sup>15</sup>N-, and <sup>13</sup>C-labeled samples. Sequential backbone assignments were obtained manually using <sup>1</sup>H-<sup>15</sup>N HSQC, HNCACB, and CBCA(CO)NH experiments (20, 21). NMR data were processed with NMRPipe (22) and visualized in NMRDraw (23) and NMRView (24).

**NMR Peptide Titration Studies**—Titration experiments of unlabeled peptide into a sample containing uniformly <sup>15</sup>N-labeled protein were performed by acquisition of <sup>1</sup>H-<sup>15</sup>N HSQC spectra at various peptide/protein ratios. Initially, a <sup>1</sup>H-<sup>15</sup>N HSQC spectrum of protein at ~0.16 mM concentration was recorded in the absence of peptide. The 350-μl sample was then removed from the NMR tube and mixed with 14 μl of 2 mM peptide solution to achieve a peptide/protein molar ratio of 0.5:1. The mixed sample was returned to the NMR tube, and a new <sup>1</sup>H-<sup>15</sup>N HSQC spectrum was recorded. More peptide solution was incrementally added to acquire <sup>1</sup>H-<sup>15</sup>N HSQC spectra

## Crystal Structure of IP<sub>3</sub>R3 Suppressor Domain

at peptide/protein molar ratios of 1:1, 2:1, and 3:1. The reported results are for the spectra measured in the absence of peptide compared with the presence of a 3-fold molar excess of peptide. Data were analyzed by first normalizing raw peak volumes with the peak volume of a reference peak (peak unaffected by peptide addition) in the same spectrum. The peak volume values were then compared between the no-peptide and 3-fold molar excess peptide-added conditions.

**GST Pull-down Assays**—GST-T3S4S5 and GST-T1S4S5 (pGEX-4T vectors (GE Healthcare)) were expressed as described above. Suppressor domain proteins were subcloned into pET28-a expression vectors (Novagene) and expressed as N-terminal His fusion proteins in BL21-CodonPlus(DE3)-RIL *E. coli* strain (Stratagene) in 1 liter of LB medium grown at 15 °C overnight after induction with 0.5 mM IPTG (final concentration). Harvested cells were lysed in buffer (20% (v/v) glycerol, 20 mM Tris-HCl, pH 7.1, 500 mM NaCl, 20 mM imidazole, 0.2% Nonidet P-40, 10 μg/ml DNase I, EDTA-free protease inhibitor mixture (Roche Applied Science), 0.5 mM TCEP), and the clarified supernatant was subjected to affinity chromatography by passing it through a pre-equilibrated nickel-NTA resin (Qiagen). After washing with 3 column volumes of wash buffer (10% (v/v) glycerol, 20 mM Tris-HCl, pH 7.1, 300 mM NaCl, 20 mM imidazole, 0.5 mM TCEP), the His fusion proteins were eluted in buffer containing 3% (v/v) glycerol, 20 mM Tris-HCl, pH 7.1, 300 mM NaCl, 300 mM imidazole, 0.5 mM TCEP and dialyzed against the incubation buffer, which is identical in composition to the NMR titration buffer (3% (v/v) glycerol, 20 mM Tris-HCl, pH 7.1, 300 mM NaCl, 2 mM TCEP). Prior to incubation with suppressor domain proteins, the GST columns with immobilized GST-T3S4S5 or GST-T1S4S5 were pre-equilibrated with incubation buffer. The bed volume of the GST column was 250 μl. 500 μg of purified IP<sub>3</sub>R1<sub>SUP</sub> or IP<sub>3</sub>R3<sub>SUP</sub> were incubated with 200 μg of GST fusion proteins in the column for 2 h at 4 °C. Following five 1-ml washes with high salt buffer (3% (v/v) glycerol, 15 mM Tris-HCl, pH 7.1, 500 mM NaCl, 2 mM TCEP), proteins were eluted using 250 μl of elution buffer (50 mM Tris-HCl, pH 7, 300 mM NaCl, 10 mM DTT, and 10 mM reduced glutathione). The 30 μl of elution samples were separated on a 15% SDS-polyacrylamide gel and then analyzed by Western blotting using a 1:1000 dilution of a primary penta-His antibody (Qiagen). Bands were quantitated by a densitometer, and controls were normalized to 1.

## RESULTS

**Crystal Structure of the Type 3 IP<sub>3</sub>R Suppressor Domain**—The three-dimensional structure of IP<sub>3</sub>R3<sub>SUP</sub> consists of a hammer-like overall shape with a globular “head” domain comprising a β-trefoil fold and a helix-turn-helix motif, which makes up the “arm” domain (Fig. 1 and Table 1). The overall structure of IP<sub>3</sub>R3<sub>SUP</sub> superimposes very well with that of IP<sub>3</sub>R1<sub>SUP</sub> reported previously (root mean square deviation ~1.3 Å) (Fig. 1B) (25). The 12-β-strand β-trefoil fold of IP<sub>3</sub>R3<sub>SUP</sub> is characterized by three trefoils, which together form a barrel and cap structure. Each trefoil is made up of two two-stranded hairpins, with one hairpin contributing to the barrel structure and the

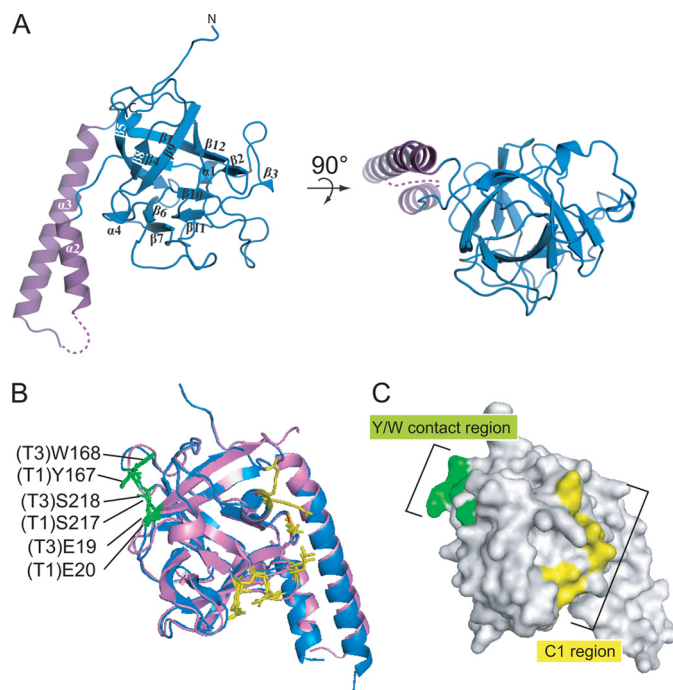


**FIGURE 1. Crystal structure of IP<sub>3</sub>R3<sub>SUP</sub>.** *A*, ribbon diagram of mouse IP<sub>3</sub>R3<sub>SUP</sub>. The overall hammer-like structure consists of two subdomains; the β-trefoil head subdomain is displayed in blue, and the helix-turn-helix Arm subdomain is shown in purple. Dotted lines, missing residues. *B*, superposition of IP<sub>3</sub>R3<sub>SUP</sub> (blue) and IP<sub>3</sub>R1<sub>SUP</sub> (violet; Protein Data Bank code 1XZZ) structures. T1, IP<sub>3</sub>R1; T3, IP<sub>3</sub>R3. Residues implicated in M4-M5 linker interaction and critical for IP<sub>3</sub> suppression are shown as sticks and highlighted in green and yellow, respectively. *C*, surface representation of IP<sub>3</sub>R3<sub>SUP</sub>. Tyr/Trp (Y/W) contact region and C1 region are colored green and yellow, respectively.

**TABLE 1**

**Data collection and refinement statistics for IP<sub>3</sub>R3<sub>SUP</sub> structure**

Parameter	Value
<b>Data collection</b>	
Space group	C2
Cell parameters	a = 79.4 Å, b = 59.9 Å, c = 111.4 Å, β = 97.88°
Wavelength (Å)	0.9792
Resolution (Å)	50.0-1.9
Completeness (%)	99.8 (100.0) <sup>a</sup>
Redundancy	3.6 (3.6)
R <sub>sym</sub> (I) (%)	7.8 (39.0)
Data with I > 2σ(I) (%)	81.5 (52.3)
<b>Refinement</b>	
R <sub>cryst</sub> (%)	21.6
R <sub>free</sub> (%)	25.2
Total no. of atoms	3651
Deviations, bond lengths (Å)	0.005
Deviations, bond angles (degrees)	1.3
Mean B factors, proteins (Å <sup>2</sup> )	25.1
Mean B factors, solvent (Å <sup>2</sup> )	25.2
Residues in most favored regions (%)	90.3
Residues in additionally allowed regions (%)	9.7
Residues in generously allowed regions (%)	0
Residues in disallowed regions (%)	0

<sup>a</sup> Highest resolution shell is shown in parentheses.

other forming the cap structure. Poorly defined electron density prevented us from modeling one stretch of the protein that is a part of the arm domain (Gln-76 to Glu-82).

**Structural Comparisons with Type 1 IP<sub>3</sub>R Suppressor Domain and Implications for Isoform-specific IP<sub>3</sub> Binding Affinity**—To understand the molecular basis of isoform-specific IP<sub>3</sub> binding affinity, we performed a careful inspection of the structures of IP<sub>3</sub>R3<sub>SUP</sub> and IP<sub>3</sub>R1<sub>SUP</sub>. Comparison of IP<sub>3</sub>R3<sub>SUP</sub> and IP<sub>3</sub>R1<sub>SUP</sub>

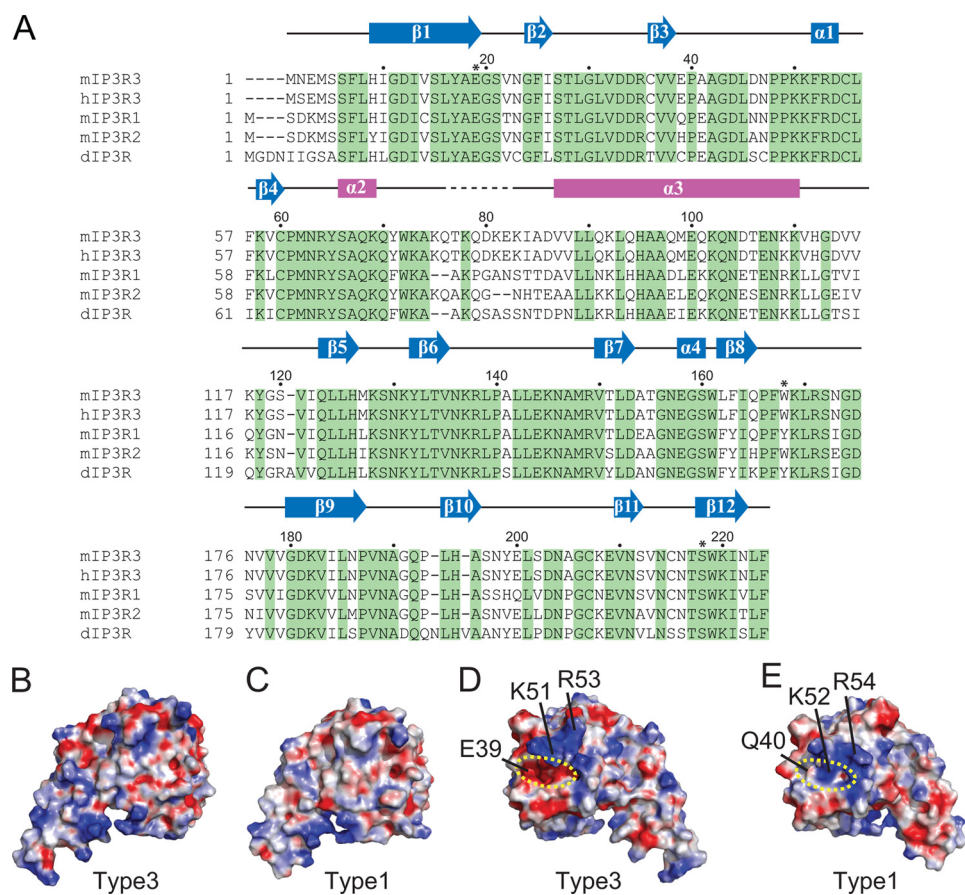


**FIGURE 2. Sequence alignment of members of the IP<sub>3</sub>R family and electrostatic surface potential diagrams of crystal structures of type 1 and 3 IP<sub>3</sub>R suppressor domain.** A, sequence alignment with conserved residues highlighted in green (accession numbers: mIP<sub>3</sub>R3, NP\_542120.2; hIP<sub>3</sub>R3, NP\_002215.2; mIP<sub>3</sub>R1, NP\_034715.3; mIP<sub>3</sub>R2, NP\_064307.2; dIP<sub>3</sub>R, NP\_730942.1). Secondary structural elements of mIP<sub>3</sub>R3<sub>SUP</sub> identified from the crystal structure are displayed:  $\beta$ -strands as arrows and  $\alpha$ -helices as rectangles (a dotted line represents the unresolved portion). Structural elements from the head subdomain are colored blue, and those from the arm subdomain are colored purple. Asterisks denote residues involved in M4-M5 linker interaction. Surface electrostatics of IP<sub>3</sub>R3<sub>SUP</sub> (B and D) and of IP<sub>3</sub>R1<sub>SUP</sub> (C and E) are shown. The acidic patch of IP<sub>3</sub>R3<sub>SUP</sub> and the corresponding area on IP<sub>3</sub>R1<sub>SUP</sub> are highlighted (yellow dotted oval). Views in D and E are 180° rotated along the y axis with respect to those in B and C, respectively.

surface electrostatic potential maps reveals several significant differences. First, IP<sub>3</sub>R3<sub>SUP</sub> possesses a highly acidic pocket, whereas the corresponding region in IP<sub>3</sub>R1<sub>SUP</sub> is more positively charged (Fig. 2, B–E). This difference is attributed to an anionic residue in IP<sub>3</sub>R3 (Glu-39), which is replaced with glutamine (Gln-40) in IP<sub>3</sub>R1<sub>SUP</sub>. The other residue that contributes to the electrostatics of this region is the basic residue Arg-54 in IP<sub>3</sub>R1<sub>SUP</sub>, or Arg-53 in IP<sub>3</sub>R3<sub>SUP</sub>. The side chain of Arg-54 in IP<sub>3</sub>R1<sub>SUP</sub> is positioned on the surface to exclusively cover the underlying pocket (Fig. 2E). In contrast, the side chain of Arg-53 in IP<sub>3</sub>R3<sub>SUP</sub> protrudes away from the pocket and is largely exposed to the solvent. The two suppressor domains also display differences in the surface electrostatics of their arm domains. Overall, the arm domain of IP<sub>3</sub>R3<sub>SUP</sub> is more neutral, whereas in IP<sub>3</sub>R1<sub>SUP</sub> this region is more acidic. The difference in the orientation of the Arg-53 side chain and the presence of Glu-39 in IP<sub>3</sub>R3<sub>SUP</sub> may contribute to isoform-specific IP<sub>3</sub> binding affinity. It should be noted that this region coincides with a highly conserved region within the suppressor domain, previously named the C1 region (aa Ser-28 to Arg-36, Pro-49 to Leu-57, Cys-61 to Gln-71, Gln-122 to Asp-152, and Gly-155 to

Gly-158 of mouse IP<sub>3</sub>R1) (25). The high amino acid conservation of this region, combined with site specific charge variation, is consistent with an IP<sub>3</sub> binding modulation property common to all IP<sub>3</sub>R isoforms. Indeed, the C1 region contains many residues previously identified by mutagenesis to be critical for suppression of IP<sub>3</sub> binding (Fig. 5) (25). The sole residue that is not strictly conserved in this region is Met-127 (Leu-126 in type 1), which, among others, has been previously implicated to have a role in modulating IP<sub>3</sub>R3-specific IP<sub>3</sub> binding affinity (9).

Whereas the IP<sub>3</sub>R1<sub>SUP</sub> crystal contained only one molecule in the asymmetric unit, the IP<sub>3</sub>R3<sub>SUP</sub> crystal contained two molecules (supplemental Fig. 2) with a buried surface area of ~1617 Å<sup>2</sup>. This marked interaction surface is stabilized by multiple forces (supplemental Fig. 3). Specifically, residues Trp-161, Phe-163, and Val-188 from molecule A and residues Met-127, Ile-13, and Phe-224 from molecule B are involved in the hydrophobic interaction (supplemental Fig. 3). Arg-53 of molecule A forms a salt bridge with Glu-107 of molecule B and also interacts with residue Asn-104. We observe hydrogen bonds between two asparagine residues (Asn-130 from molecule A and Asn-173 from

molecule B). Of the 11 residues contributing to the interface, three are unique to the type 3 isoform (Met-127, Phe-163, and Asn-173). The most pronounced difference is that the isoleucine that exists in type 1 is replaced by Asn-173 in the aligned position of the type 3 isoform. Less dramatic substitutions are tyrosine and isoleucine residues in type 1 IP<sub>3</sub>R for Phe-163 and Met-127, respectively, in the type 3 isoform.

*In Vitro Interaction between the Suppressor Domain and the M4-M5 Linker*—Previous reports have shown a direct interaction between the N-terminal 42-kDa and C-terminal 94-kDa fragments of IP<sub>3</sub>R (11). More recently, a 20-amino acid stretch between transmembrane helices 4 and 5, the M4-M5 linker, has been implicated in this N-C termini interaction (N-C interaction) (12). Notably, mutations to the M4-M5 linker that perturb its interaction with the N-terminal fragment result in a non-functional channel (12). Based on these pioneering studies, we sought specific amino acids within the suppressor domain, which can interact with the M4-M5 linker. In our accompanying study (31), we observed that mutation to a single residue (Tyr-167 or Trp-168 in type 1 or type 3 IP<sub>3</sub>R, respectively) was sufficient to abolish channel activity.

## Crystal Structure of IP<sub>3</sub>R3 Suppressor Domain

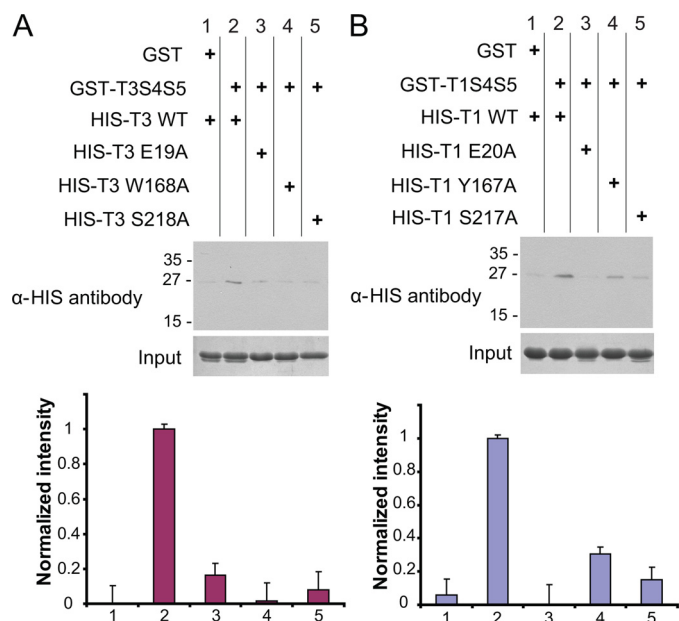


**FIGURE 3. GST pull-down assays of M4-M5 linker and IP<sub>3</sub>R<sub>3</sub>SUP proteins.** Interaction of wild type and mutant IP<sub>3</sub>R<sub>3</sub>SUP (A) or IP<sub>3</sub>R<sub>1</sub>SUP (B) proteins with their respective M4-M5 linkers. Bands were quantitated by a densitometer, and controls were normalized to 1. Error bars, S.E.

To examine whether the suppressor domain could interact with the M4-M5 linker *in vitro*, we performed GST pull-down assays using immobilized GST-M4-M5 linker and N-terminal His-tagged type 1 or type 3 IP<sub>3</sub>R<sub>3</sub>SUP wild type proteins as well as their respective mutant proteins, Y167A or W168A. The results show that the M4-M5 linker interacts with wild type IP<sub>3</sub>R<sub>1</sub>SUP or IP<sub>3</sub>R<sub>3</sub>SUP *in vitro* but not to the GST control (Fig. 3). The Y167A or the W168A mutant proteins, on the other hand, displayed considerably weaker binding under the same conditions (Fig. 3, lane 4). These data confirm that Tyr-167 from type 1 or Trp-168 from type 3 are critical to the N-C interaction and that mutation of this single residue is sufficient to disrupt this interaction.

**Mapping the Residues within the Suppressor Domain Responsible for Interaction with the M4-M5 Linker**—We performed NMR titrations using chemically synthesized peptides corresponding to the M4-M5 linker into <sup>15</sup>N-labeled IP<sub>3</sub>R<sub>3</sub>SUP and IP<sub>3</sub>R<sub>1</sub>SUP proteins and monitored changes to their respective <sup>1</sup>H-<sup>15</sup>N HSQC spectra. We recorded the <sup>1</sup>H-<sup>15</sup>N HSQC spectra of both IP<sub>3</sub>R<sub>1</sub>SUP (aa 1–223) and IP<sub>3</sub>R<sub>3</sub>SUP (aa 1–224). The <sup>1</sup>H-<sup>15</sup>N correlation peaks observed for IP<sub>3</sub>R<sub>1</sub>SUP were considerably broader in comparison with IP<sub>3</sub>R<sub>3</sub>SUP, which behaved well during long three-dimensional triple resonance experiments; consequently, we were able to sequentially assign ~70% of the backbone of IP<sub>3</sub>R<sub>3</sub>SUP using these data (supplemental Fig. 4).

Due to the low solubility of the chemically synthesized M4-M5 linker peptide (aa 2418–2437 in IP<sub>3</sub>R1; aa 2346–2365 in IP<sub>3</sub>R3) in aqueous solution, we utilized the half-peptides, which displayed better solubility. To identify residues involved in the N-C interaction of IP<sub>3</sub>R, we titrated either the N-terminal half (T1S4S5N, aa 2418–2427 for IP<sub>3</sub>R1; T3S4S5N, aa 2346–2355 for IP<sub>3</sub>R3) or C-terminal half (T1S4S5C, aa 2428–2437 for IP<sub>3</sub>R1; T3S4S5C, aa 2356–2365 for IP<sub>3</sub>R3) of the M4-M5 linker to IP<sub>3</sub>R<sub>1</sub>SUP or IP<sub>3</sub>R<sub>3</sub>SUP proteins (Fig. 4 and supplemental Fig.

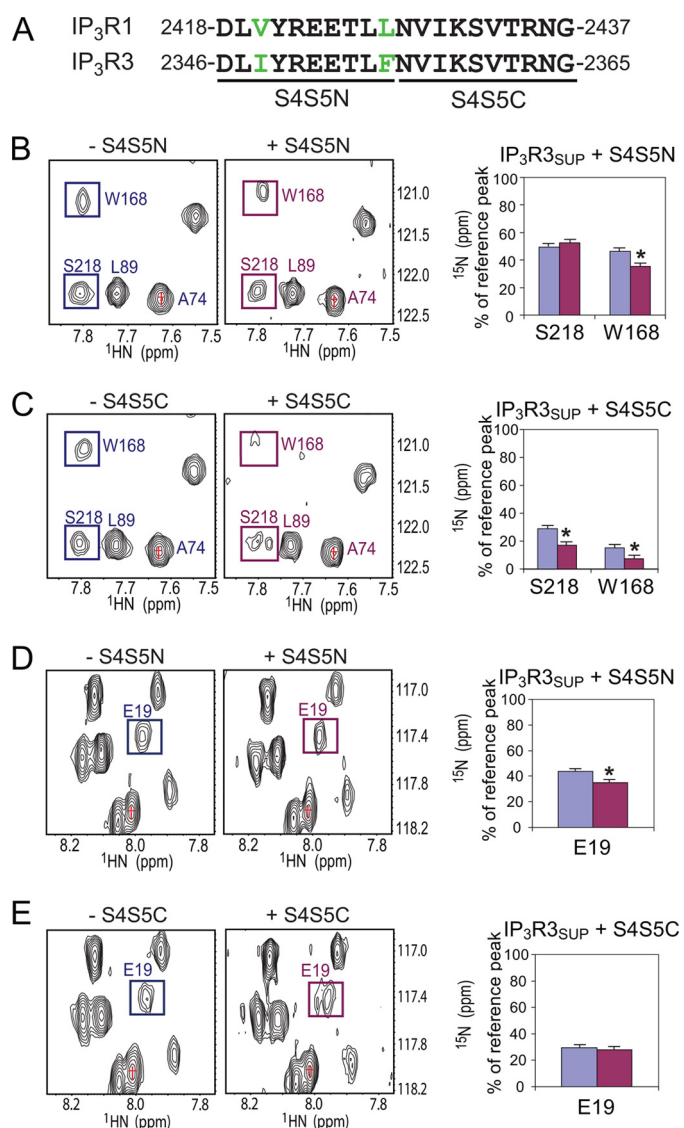


**FIGURE 4. NMR titration of M4-M5 linker peptides into <sup>15</sup>N-labeled IP<sub>3</sub>R<sub>3</sub>SUP.** A, sequence of M4-M5 linker region from type 1 and 3 IP<sub>3</sub>R. B and C, the HSQC spectrum region bound by 7.50–7.89 ppm in the <sup>1</sup>H<sub>N</sub> dimension and 120.5–122.5 ppm in the <sup>15</sup>N dimension. D and E, the HSQC spectrum region within 7.78–8.27 ppm in the <sup>1</sup>H<sub>N</sub> dimension and 116.9–118.2 ppm in the <sup>15</sup>N dimension. Titration experiments were performed by the addition of peptides corresponding to the N-terminal half (S4S5N) (B and D) or C-terminal half (S4S5C) (C and E) of the M4-M5 linker. In B, a region of the HSQC spectrum of wild type IP<sub>3</sub>R<sub>3</sub>SUP before the addition of S4S5N peptide (top left panel) is compared with the spectrum after the addition of a 3-fold molar excess of S4S5N (top center). Peak volumes of boxed resonance peaks (relative to a reference peak labeled with a red cross) are plotted in the bar graph (top far right). Blue bars, no peptide added; pink bars, a 3-fold molar excess of peptide added. \*, a ≥20% decrease in peak volume upon the addition of peptide. Error bars, S.E.

5). We recorded <sup>1</sup>H-<sup>15</sup>N HSQC spectra of IP<sub>3</sub>R<sub>3</sub>SUP or IP<sub>3</sub>R<sub>1</sub>SUP with successive additions of each peptide at peptide/protein ratios of 0.5:1, 1:1, 2:1, and 3:1. For IP<sub>3</sub>R<sub>3</sub>SUP, at low peptide/protein molar ratios (*i.e.* less than 1:1), no significant change was observed. However, at molar ratios of 1:1 or above, peak broadening was notable for a number of specific residues (data not shown). By comparing peak volumes before and after a 3-fold molar excess of peptide was added, we noticed that at least three peaks (Glu-19, Trp-168, and Ser-218) showed a reduction of greater than 20% in the presence of either

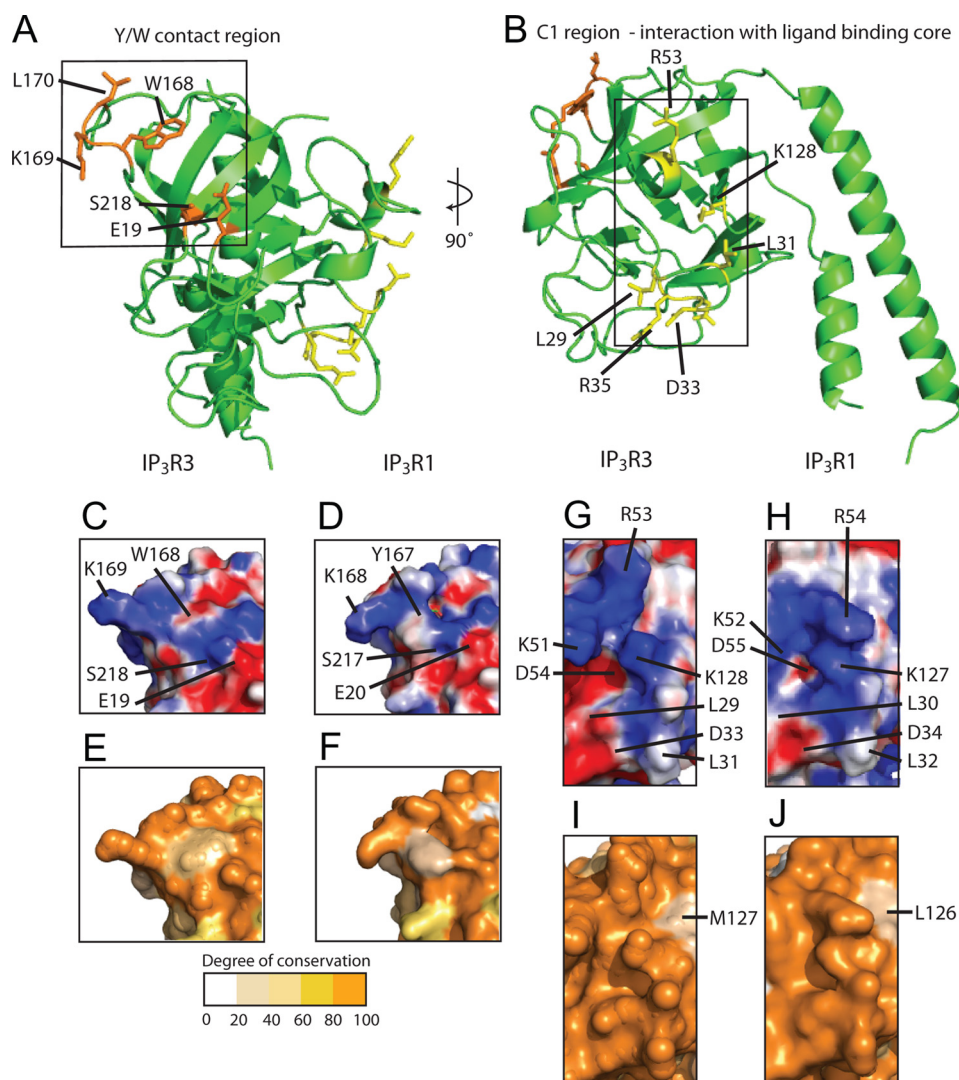


FIGURE 5. **Two distinct functional faces of IP<sub>3</sub>R<sub>3</sub><sup>SUP</sup>.** *A*, crystal structure of IP<sub>3</sub>R<sub>3</sub><sup>SUP</sup> represented as a ribbon diagram. Residues highlighted in orange represent the Tyr/Trp (Y/W) contact region. Residues colored in yellow are critical for suppression of IP<sub>3</sub> binding. *B*, same as in *A* but with 90° rotation along the y axis. *C*, the surface electrostatic potential of the boxed region in *A* of IP<sub>3</sub>R<sub>3</sub><sup>SUP</sup>. *D*, the corresponding region in IP<sub>3</sub>R<sub>1</sub><sup>SUP</sup>. *E* and *F*, conservation of IP<sub>3</sub>R<sub>3</sub><sup>SUP</sup> and IP<sub>3</sub>R<sub>1</sub><sup>SUP</sup>, respectively, within the IP<sub>3</sub>R family according to the alignment in Fig. 2. *G*, surface electrostatic potential of the boxed region in *B*. *H*, the corresponding region in IP<sub>3</sub>R<sub>1</sub>. *I* and *J*, conservation of this region for IP<sub>3</sub>R<sub>3</sub><sup>SUP</sup> and IP<sub>3</sub>R<sub>1</sub><sup>SUP</sup>, respectively.

T3S4S5N or T3S4S5C peptide. Specifically, the resonance peak corresponding to Trp-168 was broadened in the presence of either T3S4S5N or T3S4S5C peptides, whereas the Trp-19 peak volume was only reduced in the presence of T3S4S5N, and the Ser-218 peak volume was only reduced with the addition of T3S4S5C peptide. These results implicate that both N- and C-terminal halves of the M4-M5 linker are involved in the interaction with the suppressor domain. We generated E19A and S218A mutant proteins (as well as E20A and S217A mutants in type 1 IP<sub>3</sub>R<sub>SUP</sub>) and confirmed by GST pull-down assays that their absence disrupted the M4-M5 linker interaction with the suppressor domain (Fig. 3).

## DISCUSSION

IP<sub>3</sub>Rs are a tetrameric receptor with a combined molecular mass of ~1.2 MDa, whose cytoplasmic region harbors various regulatory functions of the Ca<sup>2+</sup> channel's gating. Among these

regulatory processes, such as those involving protein phosphorylation, ATP binding, interactions, with cellular proteins, IP<sub>3</sub> binding by the N-terminal region plays a crucial and universal role in the channel gating. This ligand-dependent activation is conserved among the three isoforms, but the ligand sensitivity and the channel response are different from one isoform to another. In parallel to these channel properties, these isoforms are expressed to varying degrees in different mammalian cells. IP<sub>3</sub>R1 is the major isoform expressed in the nervous system, whereas IP<sub>3</sub>R2 and IP<sub>3</sub>R3 are predominant in most other tissues. At the amino acid sequence level, the isoforms are modestly conserved, based on *Mus musculus* sequence comparisons: 68% identity between IP<sub>3</sub>R1 and IP<sub>3</sub>R2, 64% identity between IP<sub>3</sub>R1 and IP<sub>3</sub>R3, and 61% identity between IP<sub>3</sub>R2 and IP<sub>3</sub>R3. In an effort to gain insight into the general mechanism of ligand-induced gating of IP<sub>3</sub>Rs and the structural differences and similarities between the isoforms, we have investigated the structure of the suppressor domain of type 3 IP<sub>3</sub>R and the interaction of this domain with the putative binding site on the channel domain. Our structural studies presented in this paper augment the functional and biochemical data described in the accompanying paper (31), highlighting the significance of the interaction of the suppressor domain

with the channel domain in the gating function of both type 1 and type 3 IP<sub>3</sub>Rs.

Despite various EM structures of full-length IP<sub>3</sub>R, the exact positions of the suppressor domain and ligand binding domain remains ill defined. Hence, the exact orientation and distance between the suppressor domain and the M4-M5 linker are currently unknown. Our NMR titration studies identified three residues (Glu-19, Trp-168, and Ser-218) within IP<sub>3</sub>R<sub>3</sub><sup>SUP</sup> that are either directly in contact with or in close proximity to the interaction interface with the M4-M5 linker. In our accompanying paper (31), the corresponding residues (Glu-20, Tyr-167, and Ser-217) in IP<sub>3</sub>R1 have been mutated to alanine. Although single substitution at Glu-20 and Ser-217 did not show significant change in the Ca<sup>2+</sup> release activity of the channel, the E20A/Y167A/S217A triple substitution exhibited a significant change in the gating function. Moreover, this mutant displayed significantly lower sensitivity against trypsin compared with

## Crystal Structure of IP<sub>3</sub>R3 Suppressor Domain

that of Y167A. Using our Ca<sup>2+</sup> flux assays (31), we have found that Lys-168 and Leu-169 in IP<sub>3</sub>R1 were also functionally important. The corresponding residues in IP<sub>3</sub>R3 are Lys-169 and Leu-170, respectively. We mapped these conserved residues to our crystal structure of IP<sub>3</sub>R3<sub>SUP</sub> (Fig. 5) and found that they localize to one face of the head domain, on which Trp-168 is situated in the center of the binding site. Because the corresponding residue in IP<sub>3</sub>R1 is Tyr-167, we have denoted this region the Tyr/Trp contact region (Figs. 1 and 5). This M4-M5 linker binding site is distinct from the C1 region of the structure (25), which has been shown to interact with the ligand binding core domain (26). The distinction is clearly shown in the structure of IP<sub>3</sub>R3<sub>SUP</sub>, where the Tyr/Trp contact region is located at an opposite face of the C1 region (Fig. 1, B and C). The observation that the interaction of the suppressor domain with the M4-M5 linker does not mutually exclude its interaction with the core domain suggests that the two events potentially act together in a cooperative manner. Further studies are required to deduce the precise binding mechanism of the M4-M5 linker to the suppressor domain and its relationship with IP<sub>3</sub> binding. Because the structures of IP<sub>3</sub>R1<sub>SUP</sub> and IP<sub>3</sub>R3<sub>SUP</sub> are very similar, it is not surprising that the corresponding residues in the type 1 suppressor domain (Glu-20, Tyr-167, and Ser-217) are localized to the same face of the structure. Moreover, the surface electrostatic potentials of the suppressor domain (Fig. 5) and amino acid sequence of the M4-M5 linker (Fig. 4) are very similar between type 1 and type 3 IP<sub>3</sub>R, suggesting that the interaction with the M4-M5 linker is conserved between the two isoforms.

Specific mutations to either the M4-M5 linker or to the IP<sub>3</sub>R suppressor domain result in a non-functional channel (12, 31). Interestingly, we note that the IP<sub>3</sub>R gating-deficient mutation (Y167A in the type 1 isoform, W168A in the type 3 isoform) coincides with a large basic region in the N-terminal domain of type 1 ryanodine receptor (RyR1) (27) to which a “hot spot” of mutations resulting in malignant hyperthermia and/or central core disease are localized. These disease-associated mutations in RyR1 and the IP<sub>3</sub>R gating-deficient mutations are found in the loop segment between β8 and β9 (loop 8) (supplemental Fig. 6). In the case of RyR, it has been suggested that the TM6-TM7 loop (analogous to the M4-M5 linker in IP<sub>3</sub>R) interacts with a region within its central domain (28). The present experimental data from both functional and structural studies strongly argue that the suppressor domain provides a key interaction for the N-C coupling required for the ligand-operated Ca<sup>2+</sup> channel gating function of IP<sub>3</sub>Rs. The presence of other interaction points (possibly including the 160 most C-terminal residues of IP<sub>3</sub>R) between the M4-M5 linker and the cytoplasmic region of IP<sub>3</sub>R cannot be excluded.

The present study and the accompanying paper (31) have provided compelling evidence for a critical role of the IP<sub>3</sub>R suppressor domain in the channel gating function as well as the IP<sub>3</sub> sensitivity. More specifically, the Tyr/Trp contact residue (Tyr-167 in IP<sub>3</sub>R1 and Trp-168 in IP<sub>3</sub>R3) is essential in the communication between the N-terminal ligand-binding region and the C-terminal channel domain. The crystal structure of the type 3 suppressor domain revealed that this region is structurally conserved, and our NMR data suggested that these aromatic residues in type 1 and 3, together with Glu-20 and Ser-217 in type 1

and Glu-19 and Ser-218 in type 3, are involved in the interaction with the M4-M5 linker within the transmembrane domain in each isoform. Although this interaction is essential to the channel gating, we believe that the Tyr/Trp contact region is not the sole contributor to the gating mechanism. Instead, we propose that there are multiple “contact sites” between the transmembrane channel region and the rest of the molecule, which includes the central modulatory domain and the C-terminal “gatekeeper” domain. Together with the interaction involving the Tyr/Trp contact region within the N-terminal suppressor domain, other interactions involving a larger portion of the receptor must participate in this protein-protein interaction network, which positively and negatively regulate the activity of the Ca<sup>2+</sup> channel in response to various external stimuli, including the natural agonists IP<sub>3</sub> and Ca<sup>2+</sup>, ATP (29), and phosphorylation events (reviewed in Ref. 30). Further studies are needed to obtain a full picture of the protein-protein interaction network within the functional tetrameric receptor.

*Acknowledgments*—We thank the staff of 19-BM at APS and G. Seabrook for assistance with NMR data collection and P. Stathopoulos for critical comments on the manuscript.

## REFERENCES

1. Furuichi, T., Kohda, K., Miyawaki, A., and Mikoshiba, K. (1994) *Curr. Opin. Neurobiol.* **4**, 294–303
2. Patel, S., Joseph, S. K., and Thomas, A. P. (1999) *Cell Calcium* **25**, 247–264
3. Bush, K. T., Stuart, R. O., Li, S. H., Moura, L. A., Sharp, A. H., Ross, C. A., and Nigam, S. K. (1994) *J. Biol. Chem.* **269**, 23694–23699
4. De Smedt, H., Missiaen, L., Parys, J. B., Henning, R. H., Sienaert, I., Vanlingen, S., Gijssens, A., Himpens, B., and Casteels, R. (1997) *Biochem. J.* **322**, 575–583
5. Newton, C. L., Mignery, G. A., and Südhof, T. C. (1994) *J. Biol. Chem.* **269**, 28613–28619
6. Furuichi, T., Simon-Chazottes, D., Fujino, I., Yamada, N., Hasegawa, M., Miyawaki, A., Yoshikawa, S., Guénet, J. L., and Mikoshiba, K. (1993) *Receptors Channels* **1**, 11–24
7. Matsumoto, M., Nakagawa, T., Inoue, T., Nagata, E., Tanaka, K., Takano, H., Minowa, O., Kuno, J., Sakakibara, S., Yamada, M., Yoneshima, H., Miyawaki, A., Fukuuchi, Y., Furuichi, T., Okano, H., Mikoshiba, K., and Noda, T. (1996) *Nature* **379**, 168–171
8. Futatsugi, A., Nakamura, T., Yamada, M. K., Ebisui, E., Nakamura, K., Uchida, K., Kitaguchi, T., Takahashi-Iwanaga, H., Noda, T., Aruga, J., and Mikoshiba, K. (2005) *Science* **309**, 2232–2234
9. Iwai, M., Michikawa, T., Bosanac, I., Ikura, M., and Mikoshiba, K. (2007) *J. Biol. Chem.* **282**, 12755–12764
10. Iwai, M., Tateishi, Y., Hattori, M., Mizutani, A., Nakamura, T., Futatsugi, A., Inoue, T., Furuichi, T., Michikawa, T., and Mikoshiba, K. (2005) *J. Biol. Chem.* **280**, 10305–10317
11. Boehning, D., and Joseph, S. K. (2000) *EMBO J.* **19**, 5450–5459
12. Schug, Z. T., and Joseph, S. K. (2006) *J. Biol. Chem.* **281**, 24431–24440
13. Uchida, K., Miyauchi, H., Furuichi, T., Michikawa, T., and Mikoshiba, K. (2003) *J. Biol. Chem.* **278**, 16551–16560
14. Otwinowski, Z., and Minor, W. (1997) *Methods Enzymol.* **276**, 307–326
15. Brünger, A. T., Adams, P. D., Clore, G. M., DeLano, W. L., Gros, P., Grosse-Kunstleve, R. W., Jiang, J. S., Kuszewski, J., Nilges, M., Pannu, N. S., Read, R. J., Rice, L. M., Simonson, T., and Warren, G. L. (1998) *Acta Crystallogr. D Biol. Crystallogr.* **54**, 905–921
16. Emsley, P., and Cowtan, K. (2004) *Acta Crystallogr. D Biol. Crystallogr.* **60**, 2126–2132
17. Baker, N. A., Sept, D., Joseph, S., Holst, M. J., and McCammon, J. A. (2001) *Proc. Natl. Acad. Sci. U.S.A.* **98**, 10037–10041

18. Ikura, M., Kay, L. E., and Bax, A. (1990) *Biochemistry* **29**, 4659–4667
19. Yamazaki, T., Lee, W., Arrowsmith, C., Muhandiram, D. R., and Kay, L. E. (1994) *J. Am. Chem. Soc.* **116**, 11655–11666
20. Grzesiek, S., and Bax, A. (1993) *J. Biomol. NMR* **3**, 185–204
21. Wang, A. C., Lodi, P. J., Qin, J., Vuister, G. W., Gronenborn, A. M., and Clore, G. M. (1994) *J. Magn. Reson. B* **105**, 196–198
22. Delaglio, F., Grzesiek, S., Vuister, G. W., Zhu, G., Pfeifer, J., and Bax, A. (1995) *J. Biomol. NMR* **6**, 277–293
23. Delaglio, F. (1995) *NMRDraw*, National Institutes of Health Laboratory of Chemical Physics, Bethesda, MD
24. Johnson, B. A., and Blevins, R. A. (1994) *J. Biomol. NMR* **4**, 603–614
25. Bosanac, I., Yamazaki, H., Matsu-Ura, T., Michikawa, T., Mikoshiba, K., and Ikura, M. (2005) *Mol. Cell* **17**, 193–203
26. Bosanac, I., Alattia, J. R., Mal, T. K., Chan, J., Talarico, S., Tong, F. K., Tong, K. I., Yoshikawa, F., Furuichi, T., Iwai, M., Michikawa, T., Mikoshiba, K., and Ikura, M. (2002) *Nature* **420**, 696–700
27. Amador, F. J., Liu, S., Ishiyama, N., Plevin, M. J., Wilson, A., MacLennan, D. H., and Ikura, M. (2009) *Proc. Natl. Acad. Sci. U.S.A.* **106**, 11040–11044
28. Hamada, T., Bannister, M. L., and Ikemoto, N. (2007) *Biochemistry* **46**, 4272–4279
29. Foskett, J. K., White, C., Cheung, K. H., and Mak, D. O. (2007) *Physiol. Rev.* **87**, 593–658
30. Vanderheyden, V., Devogelaere, B., Missiaen, L., De Smedt, H., Bultynck, G., and Parys, J. B. (2009) *Biochim. Biophys. Acta* **1793**, 959–970
31. Yamazaki, H., Chan, J., Ikura, M., Michikawa, T., and Mikoshiba, K. (2010) *J. Biol. Chem.* **285**, 36081–36091